



RESEARCH ARTICLE | NOVEMBER 14 2022

# Architected frames for elastic wave attenuation: Experimental validation and local tuning via affine transformation <sup>F</sup>

Giulia Aguzzi ; Henrik R. Thomsen; Aida Hejazi Nooghabi; Richard Wiltshaw; Richard V. Craster ; Eleni N. Chatzi; Andrea Colombi

 Check for updates

*Appl. Phys. Lett.* 121, 201702 (2022)

<https://doi.org/10.1063/5.0119903>

  
View  
Online

  
Export  
Citation

CrossMark

## Articles You May Be Interested In

On the elastodynamic properties of octet truss-based architected metamaterials

*Appl. Phys. Lett.* (April 2023)

Ultra-stiff and ultra-light architected metamaterial for vibration mitigation

*J Acoust Soc Am* (October 2022)

Independence of the architect online

*AIP Conference Proceedings* (May 2023)

### 500 kHz or 8.5 GHz? And all the ranges in between.

Lock-in Amplifiers for your periodic signal measurements



Find out more



# Architected frames for elastic wave attenuation: Experimental validation and local tuning via affine transformation

Cite as: Appl. Phys. Lett. **121**, 201702 (2022); doi: [10.1063/5.0119903](https://doi.org/10.1063/5.0119903)

Submitted: 10 August 2022 · Accepted: 25 October 2022 ·

Published Online: 14 November 2022




View Online



Export Citation



CrossMark

Giulia Aguzzi,<sup>1,a)</sup>  Henrik R. Thomsen,<sup>1</sup> Aida Hejazi Nooghabi,<sup>1</sup> Richard Wiltshaw,<sup>2</sup> Richard V. Craster,<sup>2,3,4</sup>  Eleni N. Chatzi,<sup>1</sup> and Andrea Colombi<sup>1</sup>

## AFFILIATIONS

<sup>1</sup>Department of Civil, Environmental and Geomatic Engineering, ETH Zürich, Zürich 8093, Switzerland

<sup>2</sup>Department of Mathematics, Imperial College London, London SW7 2AZ, United Kingdom

<sup>3</sup>Department of Mechanical Engineering, Imperial College London, London SW7 2AZ, United Kingdom

<sup>4</sup>Abraham de Moivre-CNRS IRL, Imperial College London, London SW7 2AZ, United Kingdom

<sup>a)</sup>Author to whom correspondence should be addressed: [aguzzi@ibk.baug.ethz.ch](mailto:aguzzi@ibk.baug.ethz.ch)

## ABSTRACT

We experimentally demonstrate the capability of architected plates, with a frame-like cellular structure, to inhibit the propagation of elastic flexural waves. By leveraging the octet topology as a unit cell to design the tested prototypes, a broad and easy-to-tune bandgap is experimentally generated. The experimental outcomes are supported by extensive numerical analyses based on 3D solid elements. Drawing from the underlying dynamic properties of the octet cell, we numerically propose a tailorable design with enhanced filtering capabilities. We transform the geometry of the original unit cell by applying a uniaxial scaling factor that, by breaking the in-plane symmetry of the structure, yields independently tuned struts and consequently multiple tunable bandgaps within the same cell. Our findings expand the spectrum of available numerical analyses on the octet lattice, taking it a significant step closer to its physical implementation. The ability of the octet lattice to control the propagation of flexural vibrations is significant within various applications in the mechanical and civil engineering domains, and we note such frame-like designs could lead to advancements in energy harvesting and vibration protection devices (e.g., lightweight and resonance-tunable absorbers).

© 2022 Author(s). All article content, except where otherwise noted, is licensed under a Creative Commons Attribution (CC BY) license (<http://creativecommons.org/licenses/by/4.0/>). <https://doi.org/10.1063/5.0119903>

Architected metastructures are engineered composites, exhibiting exotic behaviors<sup>1–4</sup> tied to homogenized effective properties<sup>5</sup> of their design.<sup>6,7</sup> Such advanced mechanical and dynamic behaviors emerge from careful customization of their cellular architecture as proved, for instance, by hierarchical designs able to convey improved thermal resistance,<sup>8</sup> ultralightweight and recoverability,<sup>9</sup> or enhanced vibration attenuation performance.<sup>10</sup> Among these unique features, the so-called bandgap,<sup>11</sup> a prohibited frequency range, which has so far enabled the attenuation of waves at diverse length scales,<sup>12–15</sup> is unquestionably the most popularly exploited for architected dynamical systems. The advent of these structured materials has laid the foundations for a new realm of innovative metamaterials-based technologies,<sup>16–18</sup> such as metaplates for vibration suppression,<sup>19,20</sup> while simultaneously shedding light on a spectrum of new challenges to tackle. The most significant pertains to obtaining an easy-to-tune, wide, and low-frequency stop band in

metastructures of practically feasible size to be deployed for elastic wave mitigation. To address this requirement, several solutions have thus far been proposed,<sup>21–23</sup> such as combining the two primordial bandgap generating mechanisms, local resonance, and Bragg scattering.<sup>24,25</sup>

Local resonances, arising from the hybridization of propagating waves interacting with arrangements of resonating elements, underpin the optimal principle for designing frequency-tailorable gaps with narrow bandwidth. Combining Bragg scattering with local resonances generates broader bandgaps; however, a careful choice of lattice constant<sup>24</sup> is often required for such a coalescence to occur. The synthesis of these mechanisms can be attained from frame-like periodic lattices,<sup>26,27</sup> upon appropriate design,<sup>28</sup> created by networks of structural components, e.g., beams or plates.

Among these, our recent numerical study<sup>29</sup> has drawn attention to the octet topology [reported in Fig. 1(a)], as cellular architecture of

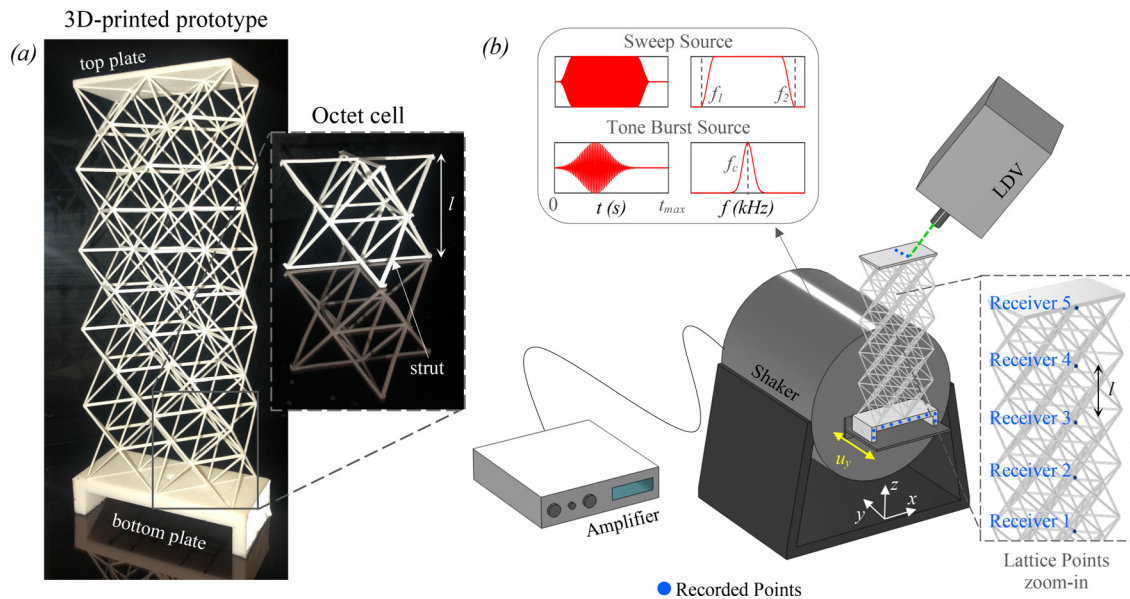


**FIG. 1.** (a) 3D-printed prototype of the standard octet-based plate. The inset shows the constitutive octet unit considered for the numerical analysis with Bloch theory. (b) Schematic of the experimental setup.

a lattice plate, for its potential in manipulating propagating elastic waves via a broadband. The complex structure of this lattice, typified by arrays of quasi-clamped<sup>30</sup> intertwined struts, supports bending resonances of its beam-like elements at selected frequencies. These resonances can be effectively leveraged to localize vibrational energy and prevent its transmission or to tune the phase velocity of waves and manipulate their trajectories. Moreover, within such periodic arrays of octet cells, Bragg scattering naturally coalesces with the fundamental flexural resonance of the underlying struts—whose wavelength matches twice the modulus of the primitive lattice vectors<sup>29,30</sup>—leading to a much wider attenuation zone than those normally anticipated from standard Fano-like interferences.<sup>31</sup>

Typically, analyses concerning frame-like periodic lattices focus on the performance of primitive cells,<sup>32</sup> or how perturbations<sup>33</sup> influence dispersive properties, usually disregarding the strut joint effect.<sup>34</sup> While this assumption is reasonable for subwavelength scattering, in the context of our previous study,<sup>29</sup> merely based on the simplified Euler–Bernoulli beam assumption, choice of model and how this affects the interaction of struts prove to be important for accurately describing the dynamics of the octet, especially when operating at the Bragg scale. Moreover, the experimental validation of this lattice has been pursued in very limited investigations,<sup>35–37</sup> with objectives outside the field of elastic wave control.

The aim of this study is to experimentally demonstrate the octet’s wave filtering performance, thereby validating our claims in Aguzzi *et al.*<sup>29</sup> by focusing on the dispersive nature of the octet, the physics underlying its attenuation mechanism, and the most relevant of its tuning parameters, i.e., added masses. Furthermore, we propose an octet design based on affine transformations of the standard cell that yield multiple bandgaps within the structure by assigning different lengths (and hence different resonances) to the underlying struts.

We begin by testing the small-scale prototype depicted in Fig. 1(a) comprising of  $2 \times 1 \times 5$  octet cells, each with size  $l = 3$  cm and containing struts with circular cross section of diameter  $t_{strut} = 1$  mm (see inset). This structure, representing a frame stemming from the periodical tessellation of the octet cell along the  $x$  and  $z$  directions, will be referred to as the *standard* octet plate, to distinguish it from its customized variant with added masses. The specimen is fabricated via Selective Laser Sintering (SLS) in versatile plastic, with nominal Young’s modulus  $E_0 = 1.7$  GPa, density  $\rho_0 = 930$  kg/m<sup>3</sup>, and Poisson ratio  $\nu_0 = 0.394$ . Two solid plates,  $6.1 \times 3.1$  cm<sup>2</sup> wide and, respectively, 2 and 5 mm thick, are 3D-printed at the top and bottom of the reticulated structure to facilitate loading and scanning.

Figure 1(b) illustrates the experimental setup (see the [supplementary material](#)), where the structure is excited by purely  $y$ -wise vibrations, generating flexural waves propagating in the  $z$  direction; these are the easiest waves to activate and carry the most energy and, hence, are the focus of our study. The wavefield is acquired using a three-component Polytec Laser Doppler Vibrometer, configured to record the horizontal velocity,  $v_y$ . To examine the wave transmission across the structure, we initially excite it with a broadband modulated sweep input at constant amplitude approximately from 1 to 6 kHz and duration  $t_{max} = 4$  s. We then measure the velocity field at the top,  $v_{y,top}$ , and bottom of the prototype,  $v_{y,bot}$ , as specified by the blue dots in Fig. 1(b). The transmission plot (gray line) in Fig. 2(a) represents the ratio of the transmitted ( $\overline{V_{y,top}}$ ) to input ( $\overline{V_{y,bot}}$ ) averaged spectral velocities (see the [supplementary material](#) for derivation), where we define transmission as

$$Transmission = 20 \cdot \log \left( \frac{\overline{V_{y,top}}(f)}{\overline{V_{y,bot}}(f)} \right), \quad (1)$$

where  $f$  is the frequency.

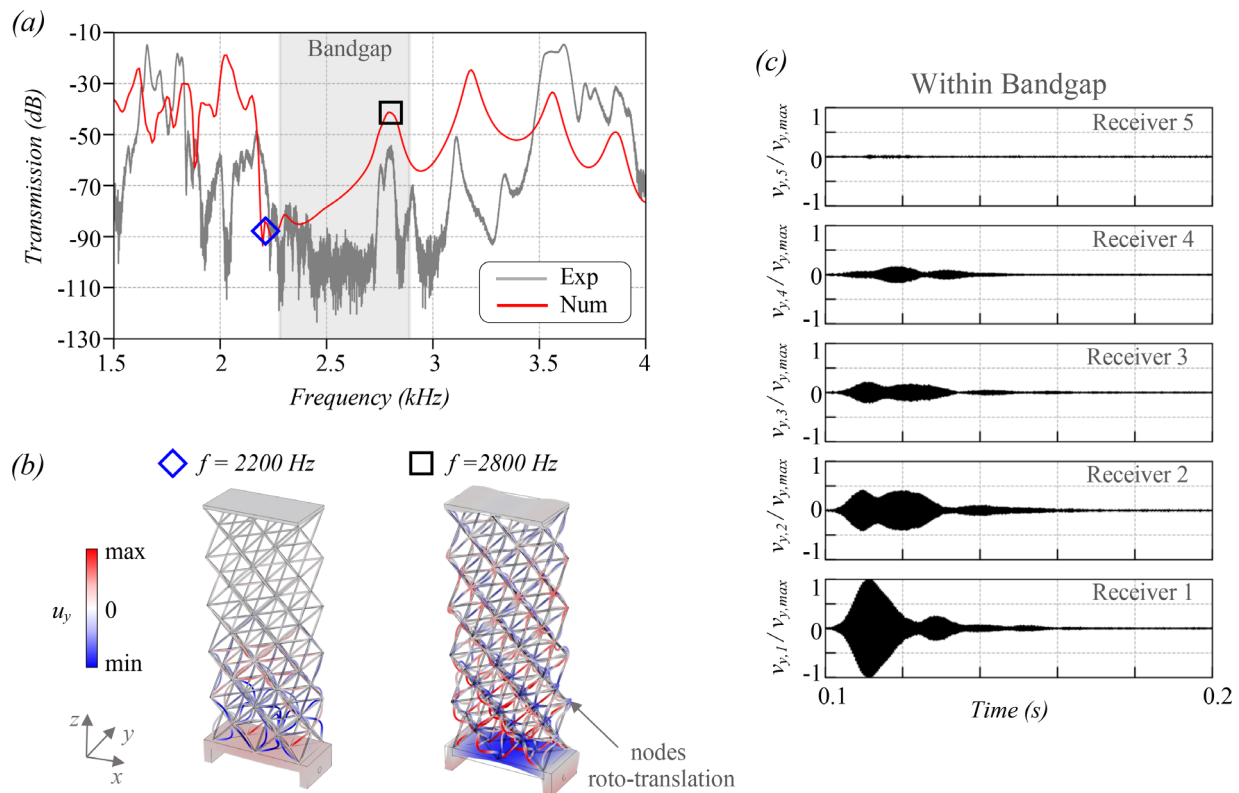


**FIG. 2.** (a) Experimental and numerical transmission spectra of the standard plate. The gray-shaded area indicates the Bloch bandgap. (b) Numerical deformation modes within (left) and after (right) the bandgap. (c) Experimental spatial amplitude decay of a narrowband velocity field along the lattice.

A drop of approximately 55 dB emerges between 2.17 and 2.75 kHz, evidence of the expected bandgap.

These results are numerically validated by the red line in Fig. 2(a), computed with a frequency domain analysis performed in COMSOL Multiphysics<sup>®</sup>. Here, the 3D-printed sample is modeled via solid tetrahedral elements. To mimic the experimental setup, we prescribe the boundary conditions  $\mathbf{u} = (0, u_y(t), 0)$  for the displacement field at the base of the structure and reproduce the experimental flat spectrum of a sweep input as in Fig. 1(b) by exciting the frame model with a time-harmonic disturbance of  $u_y(t) = u_y e^{i2\pi ft}$ , with constant amplitude  $u_y$ .

The output signals are again extracted from points on the top and bottom plates, and the transmission spectrum is computed in the same way as for the experimental data. The printing process is known to affect the material properties of the structure under investigation.<sup>38,39</sup> Thus, the numerical Young's modulus differs from  $E_0$ , which was used as an initial guess for the simulations. We found a similar discrepancy to Beli *et al.*,<sup>38</sup> where the Young's modulus of our manufactured structure was  $E = 1$  GPa—estimated by matching the numerical and experimental transmissions<sup>40</sup> (see the [supplementary material](#)). In addition, Arretche and Matlack<sup>41</sup> exposed the frequency-dependency of the experimental Young modulus in 3D printed frame lattices. This property is assumed constant in our models as we mainly focus on the experimental validation of a limited frequency range, i.e., bandgap. However, such material variability accompanied by

geometrical imperfections and anisotropy, introduced in the physical prototypes by the printing process, affects the wave propagation<sup>38,41</sup> and justifies the marginal discrepancies between the peaks and dips of numerical and experimental transmission spectra in Fig. 2(a), as also observed by Beli *et al.*<sup>38</sup> An isotropic structural loss factor  $\eta = 0.02$  was set to replicate the material damping of versatile plastic. This value was estimated by averaging the loss factors of the experimental transmission peaks surrounding the bandgap, obtained via the half-power method, and subsequently comparing it to the value used for a similar material by Beli *et al.*<sup>38</sup>

Further to corroborating the trend of its measured counterpart, the calculated transmission spectrum offers the possibility to inspect the structural deformation at selected frequencies. Among these, the vibration mode at 2.2 kHz [see Fig. 2(b)], coincident with the transmission dip that initiates the bandgap in Fig. 2(a), is of particular interest for this study as it confirms the mitigation mechanism of the octet plate. At this frequency, the local bending resonance of the constitutive struts traps the incident wavefield impeding its propagation. The energy is localized and partially dissipated by the first two rows of cells, which induce a rapid amplitude reduction toward the top of the structure. Understanding this dynamic behavior is key for unveiling the potential of the octet plate in energy harvesting applications. Indeed, the vibration energy, which is trapped and amplified by the resonance of the octet struts, could be harvested and converted into electric energy by equipping these members with piezoelectric material.<sup>42–44</sup>

Hence, the octet plate would serve as an easy-to-tailor energy harvester with lightweight design.

Conversely, at 2.8 kHz the vibration propagates across the structure, and the corresponding peak in the transmission plot designates the end of the attenuation interval. This deformation involves the roto-translation of the nodes in the lattice and matches the mode shape closing the bandgap in Aguzzi *et al.*<sup>29</sup>

The gray area in Fig. 2(a) represents the stop band prediction derived via Bloch analysis performed on a single octet cell (see the [supplementary material](#), III, for computational details). It ranges from 2.28 to 2.89 kHz, referred to as the Lower and Upper Bound Frequencies (LBF and UBF). The attenuation generated by the Bloch-gap is comparable to the one observed in the experimental and numerical spectra, even though the Bloch analysis assumes the medium is doubly periodic in the  $x$ - $z$  plane. The relative error, expressed as a percentage, between the bound frequencies (BF) of the Bloch gap and those of the attenuation zones in the numerical and experimental transmissions (TF subscripts), is estimated as follows:

$$err_{\%BF} = \frac{|BF_{\text{Bloch}} - BF_{\text{TF}}|}{BF_{\text{Bloch}}} \cdot 100\%. \quad (2)$$

The mismatches  $err_{\%LBF} = 5.7\%$  and  $err_{\%UBF} = 5.0\%$  entail a slight shift of approximately 0.1 kHz, ascribable to the influence of the boundary conditions on the dynamics of the finite system, including the additional weight due to the top plate used to collect the laboratory measurements.

After exploring the full transmission spectrum, we restrict our attention to a selected frequency within the bandgap and experimentally inspect the spatial decay of the wavefield. To this end, we excite the prototype with a narrow bandwidth input and record the  $y$ -component of the response of a line of 5 points equispaced along the lattice [see zoom-in Fig. 1(b)]. A tone burst signal with a central frequency of 2.5 kHz, 50 cycles, and lasting 1 s is employed for this purpose; the measured velocity, normalized with respect to the

maximum value of all receivers, is illustrated in Fig. 2(c). The amplitude of the signal decreases while traveling within the lattice until it ultimately reaches the top of the structure, where it approaches zero ( $v_{y,5} = 0.03v_{y,\text{max}}$ ). The velocity field halves soon after the second octet unit (receiver 2), further corroborating the reduction trend observed in the numerical deformation of Fig. 2(b) (left inset).

We now consider the customized octet plate sample depicted in Fig. 3(a). The backbone architecture of this prototype is comprised of the standard octet-like specimen in Fig. 1(a), where the midpoints of its beams are augmented by spherical added masses, denoted  $M_s$ , with diameter  $t_{\text{mass}} = 3t_{\text{strut}}$ . Both experimentally and numerically, we adopt the same approaches outlined for the standard plate. As input signal, we use a 6.25 s long sweep excitation with a flat spectrum from 1.3 to 5 kHz. The spectral transmissibility of the recorded wavefield, reported in Fig. 3(b), features a wide reduction, up to 90 dB, within the range delimited by the two peaks at 1.88 and 2.88 kHz, which indicates the predicted stop band.

The structural response is supported by numerical results in Fig. 3(b), stemming both from the frequency domain analysis conducted on the prototype solid model (red line) and the Bloch analysis on an octet cell with added masses (gray shaded region); in both cases, the Young's modulus, again obtained from the match between computational and experimental transmissibility, is 1.55 GPa (see the [supplementary material](#), for further clarification). The numerical bandgaps obtained via Bloch (1.94–2.84 kHz) and frequency-domain (1.86–2.91 kHz) analyses match the measured prediction at a maximal deviation of only 3%. The marginal discrepancies between experimental and numerical transmissibility, mainly in terms of attenuation within the stop band and at higher frequencies, can be ascribed to the material damping utilized in the numerical analyses and to the boundary conditions selected to reproduce the experimental setup, which may differ slightly from the actual configuration.

We now move to the dispersion curve engineering through geometrical modifications. To produce analyses that closely reflect the

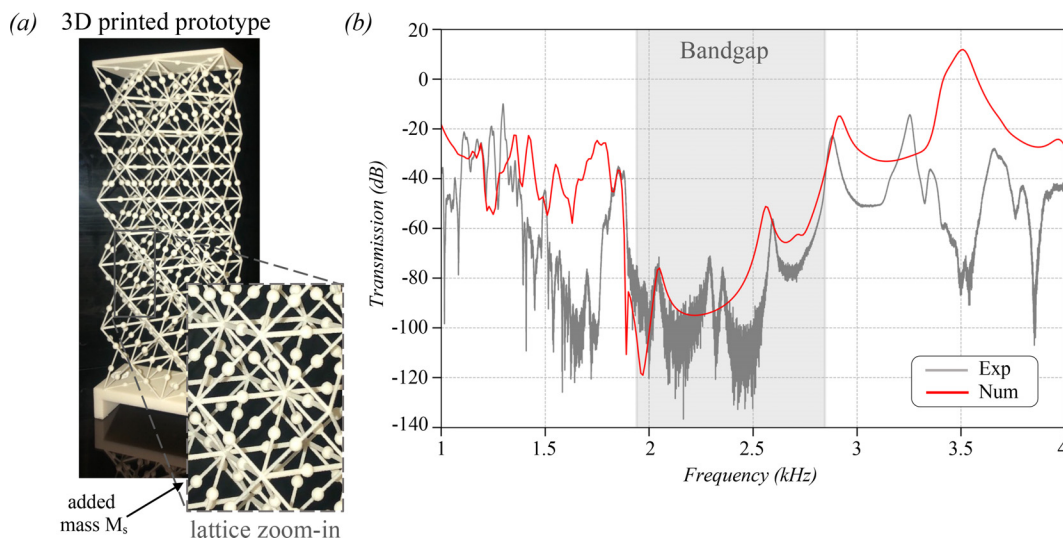


**FIG. 3.** (a) 3D-printed prototype of a customized octet plate with spherical masses added to the mid-point of the struts. (b) Experimental (gray) and numerical (red) transmission spectra of the frame in (a). The gray-shaded area defines the Bloch bandgap.

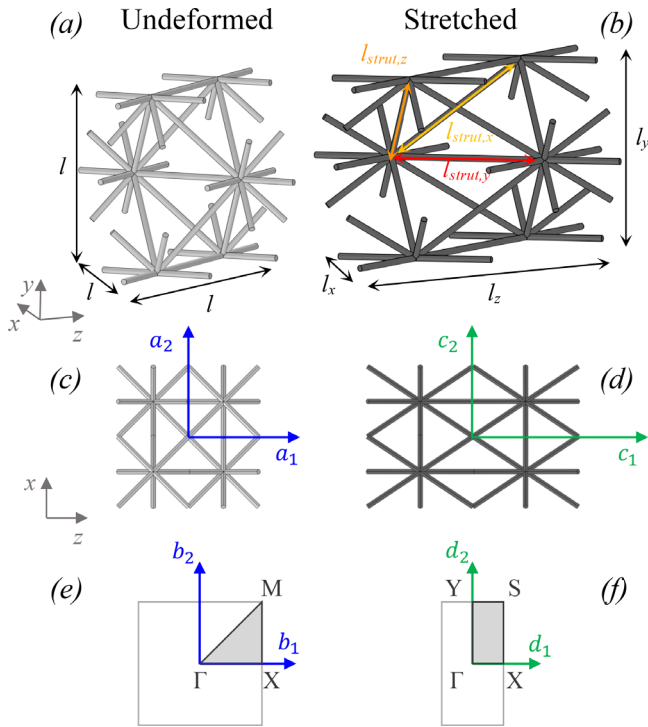


**FIG. 4.** (a) Undeformed standard octet cell, geometrically equivalent to the building block in Fig. 1(a). (b) Deformed configuration. (c) and (d) 2D view of the cells with physical lattice vectors:  $\mathbf{a}_1 = (0, 0, l)$ ,  $\mathbf{a}_2 = (l, 0, 0)$ , and  $\mathbf{c}_1 = (0, 0, l_z)$  and  $\mathbf{c}_2 = (l_x, 0, 0)$ . (e) Reciprocal lattice vectors and Irreducible Brillouin Zone of the standard octet, where  $\Gamma = (0, 0, 0)$ ,  $X = (0, 0, 1/2l)$ , and  $M = (1/2l, 0, 1/2l)$ . (f) Reciprocal lattice vectors and IBZ of the stretched octet, where  $\Gamma = (0, 0, 0)$ ,  $X = (0, 0, 1/2l_z)$ ,  $S = (1/2l_x, 0, 1/2l_z)$ , and  $Y = (1/2l_x, 0, 0)$ .

actual system, we restrict ourselves to numerical simulations based on solid 3D elements. These models, indeed, account for effects overlooked by their simplified beam-based counterparts, such as those entailed by the strut joints, as further elucidated in the [supplementary material](#). We devise a *locally tunable octet* in which the flexural resonant frequencies of its struts are independently adjusted, yielding two energy gaps in its band structure. Among potential approaches to achieve local tuning, e.g., embedding masses of different entities, we leverage an affine transformation that directionally scales the lattice periodicity while preserving the thickness of its members, namely, lattice stretching.

Lattice stretching has already been discussed in the literature, in a photonic setting to achieve unidirectional transmission<sup>45</sup> or ultra-wide Bragg-based bandgaps,<sup>46</sup> and to increase the bandwidth of topologically non-trivial bandgaps<sup>47</sup> or to investigate Bloch waves in hyperelastic stretched square lattices.<sup>48</sup> Of these, only Zhao *et al.*<sup>48</sup> consider resonance, although the resonant dynamics therein is not associated with the generation of bandgaps; instead, we leverage stretching as a flexible mechanism to achieve our ultimate goal, that is, an octet with multiple locally tunable bandgaps, induced by local resonances within struts.

We start our investigation from the undeformed cell depicted in Fig. 4(a), with equilateral edges of length  $l$  and equivalent to the building block of the standard plate, and apply an uniaxial scaling along  $z$ .

The resulting deformed octet is illustrated in Fig. 4(b). The periodicity constants of the cell are now direction-dependent and described by three parameters,  $l_x$ ,  $l_y$ , and  $l_z$ , defined as follows:

$$\begin{bmatrix} l_x \\ l_y \\ l_z \end{bmatrix} = \begin{bmatrix} S_x & 0 & 0 \\ 0 & S_y & 0 \\ 0 & 0 & S_z \end{bmatrix} \cdot \begin{bmatrix} l \\ l \\ l \end{bmatrix}, \quad (3)$$

where  $S_x$ ,  $S_y$ , and  $S_z$  are the scale factors of the 3D affine transformation matrix; when equal to 1, the deformed and undeformed configurations coincide. The full 3D symmetry of the standard octet, with identical struts of length  $l_{strut}$ , is inevitably broken when scaling the cell, assuming  $S_x \neq S_y \neq S_z$ . Consequently, three sets of beam-like elements with distinct lengths can be discerned in this structure, respectively, denoted as  $strut_x$ ,  $strut_y$ , and  $strut_z$ —where subscripts denote a *strut* whose axis is perpendicular to the appropriate Cartesian basis vector, i.e., the axis of  $strut_x$  is perpendicular to  $\mathbf{e}_x$ . Their lengths read

$$\begin{aligned} l_{strut,x} &= \sqrt{(l_y/2)^2 + (l_z/2)^2}, \\ l_{strut,y} &= \sqrt{(l_x/2)^2 + (l_z/2)^2}, \\ l_{strut,z} &= \sqrt{(l_x/2)^2 + (l_y/2)^2}. \end{aligned} \quad (4)$$

The focus here is on the transformed cell, with 12 struts of length  $l_{strut,y}$  and 8 of  $l_{strut,x}$  and  $l_{strut,z}$ , as shown in Fig. 4(b), and on its band structure computed via Bloch analysis. We define physical lattice vectors  $\mathbf{c}_1$  and  $\mathbf{c}_2$ , and reciprocal lattice vectors<sup>11</sup>  $\mathbf{d}_1$  and  $\mathbf{d}_2$  as in Fig. 4. We consider waves propagating in the  $z$  direction, again with out-of- $xz$  plane polarization, hence consider  $\mathbf{k}$  along  $\Gamma$ - $X$  (see the [supplementary material](#), for details).

Figure 5(a) outlines the dispersion relation of the transformed cell, by setting  $S_x = S_y = 1$  and  $S_z = 1.3$  in Eq. (3). Subsequently, by Eq. (4),  $l_{strut,x} = l_{strut,y}$  is increased and  $l_{strut,z}$  remains identical to the undeformed octet. The constituent beams retain their resonant behavior, inline with Eq. (S3), for beams of correct effective length (see the [supplementary material](#)), whose resonances are responsible for bandgap generation. Observe, two forbidden frequency ranges arising from the bending resonances of the struts in the lattice that, unlike those of the standard octet, are tuned to distinct frequencies. The first energy gap from 1.7 to 1.87 kHz stems from the local resonance of  $strut_x$  and  $strut_y$ , which exhibit identical resonant frequencies. The eigenmode in Fig. 5(c) at 1.7 kHz shows  $strut_z$  all stand still; indeed, their shorter length,  $l_{strut,z} = l_{strut}$ , participates in a bending mode triggering the second bandgap—which ranges from 2.22 to 2.51 kHz. The undeformed octet with isotropic symmetry and one stop band, see the [supplementary material](#), Fig. SM2, thereby evolves into a structure where its beam-like elements can be independently tuned by affine transformations, to elicit two controllable bandgaps.

Figure 5(d) shows a sensitivity analysis, to identify the scaling factor range whereby this local tuning yields the second attenuation zone. To this end,  $S_z$  is swept over the interval 0.5–2, whereas  $S_x$  and  $S_y$  are held constant to 1. For each deformed cell, the band structure is computed, and the outcome, in terms of the yielded bandgaps, is reported in Fig. 5(d). Despite the resonant mode of members  $strut_z$  animating the band diagram for all  $S_z$ , it is only for selected values that they generate the second frequency gap. This opens soon after  $S_z = 1$  and

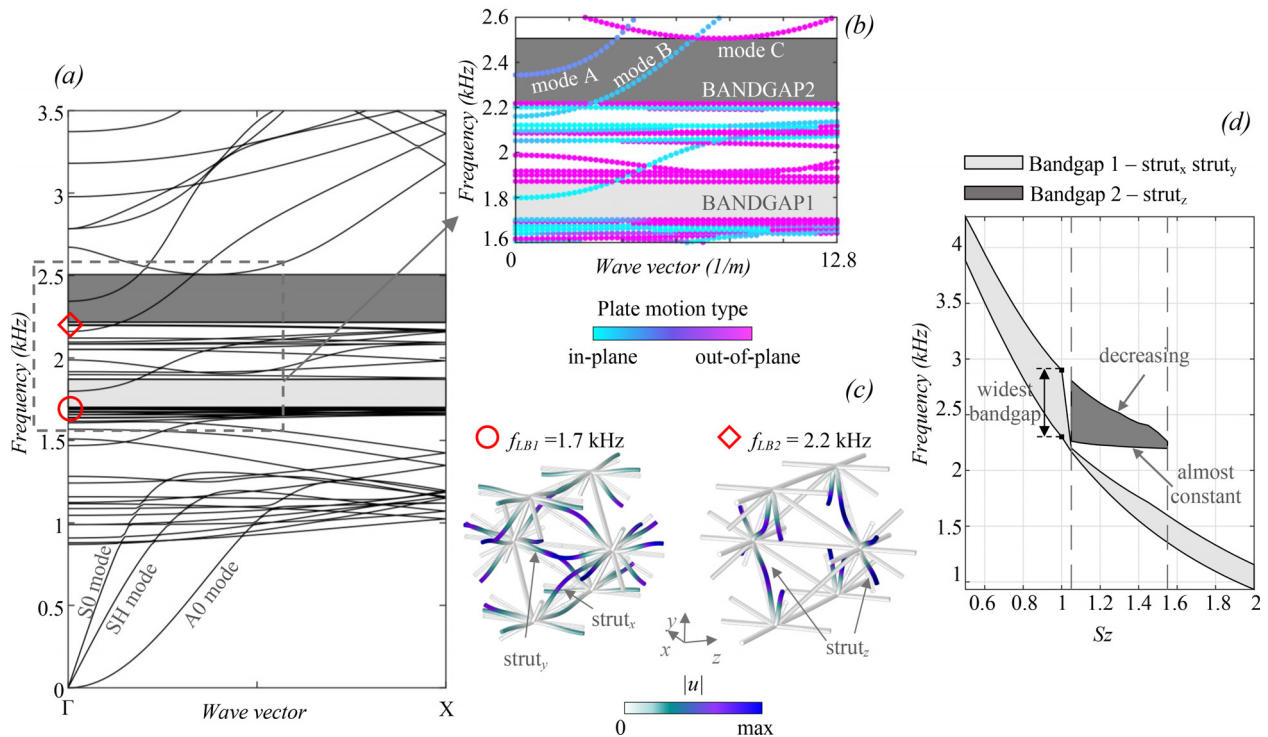


**FIG. 5.** (a) Band structure of the extended cell with  $S_x = S_y = 1$  and  $S_z = 1.3$ . (b) Zoom-in of the dispersion relation around the bandgaps, with motion polarization highlighted in color. (c) Opening mode shapes of the two bandgaps. (d) Evolution of the bandgaps as a function of the applied z-wise scaling in the tunable octet.

gradually narrows until ultimately closing around  $S_z = 1.55$ . Indeed, the resonant frequency of  $strut_z$ , that initiates the bandgap, is steady over the parametric analysis as their length is not affected by the z-wise expansion [see lower bound of bandgap 2 in Fig. 5(d)]. Conversely, the closing mode, which involves a comprehensive out-of-plane deformation of the cell, shifts to lower frequencies, owing to the softening of the structure induced by larger  $S_z$ , and eventually overlaps with the opening bound terminating the bandgap.

The undeformed octet contains the broadest bandgap; hence, for increasing  $S_z$ , smaller bandgaps and fewer frequency waves are ultimately damped. However, splitting and spreading the overall range of the attenuation zone could have its advantages regarding damping narrower band but multiple sources of vibrational energy. Moreover, since bandgap opening is still due to Eq. (S3) for constituent beams, for  $1 < S_z < 1.6$ , the dispersive branches could be tuned as required. Similar outcomes emerge when varying  $S_x$  and  $S_y$  independently, therefore omitted here.

In conclusion, our results reveal that the octet-based plate experimentally supports a broad bandgap able to inhibit the propagation of elastic Bloch waves along the host structure, provided that these lie within its frequency range, by inducing a progressive spatial decay of their amplitude. Such an exotic dynamic property creates an opportunity to enhance vibration attenuation in civil, naval, and aerospace systems, where this lightweight frame could be attached to existing structural components in order to absorb, dampen, and potentially convert their mechanical vibrations without substantially increasing their mass. The experimental results additionally validate added

masses as an effective parameter to widen and shift the energy gap while retaining the original geometry of the lattice, in terms of cell width and strut thickness.

Finally, a locally tunable octet is conceived by means of an affine transformation, where, in a specified range of the scaling factor, the struts can be selectively and independently tailored to produce two local resonance bandgaps within the same band diagram. These experimental and numerical results pave the way for the implementation of octet-based devices in vibration mitigation and extend this topology to applications that require geometric flexibility and the ability to attenuate multiple targeted frequencies.

See the [supplementary material](#) for a detailed description of the experimental and numerical analyses, and the effects of the finite element modeling technique on the octet dynamics.

G.A. and A.C. were supported by the Swiss National Science Foundation Ambizione Fellowship No. PZ00P2-174009, and G.A., A.H.N., R.V.C., and A.C. by the H2020 FETOpen project BOHEME under Grant Agreement No. 863179. H.R.T., R.W., R.V.C., and A.C. acknowledge funding from the H2020 FET-proactive project MetaVEH, European Union under the Grant Agreement No. 952039.

**AUTHOR DECLARATIONS**

**Conflict of Interest**

The authors have no conflicts to disclose.

## Author Contributions

**Giulia Aguzzi:** Conceptualization (equal); Investigation (lead); Methodology (lead); Visualization (lead); Writing – original draft (lead). **Henrik R. Thomsen:** Investigation (equal); Methodology (equal); Writing – review & editing (equal). **Aida Hejazi Nooghabi:** Investigation (equal); Methodology (equal); Writing – review & editing (equal). **Richard Wiltshaw:** Investigation (equal); Methodology (equal); Writing – review & editing (equal). **Richard V. Craster:** Investigation (equal); Supervision (equal); Writing – review & editing (equal). **Eleni N. Chatzi:** Investigation (equal); Supervision (equal); Writing – review & editing (equal). **Andrea Colombi:** Conceptualization (equal); Investigation (equal); Resources (equal); Supervision (equal); Writing – review & editing (equal).

## DATA AVAILABILITY

The data that support the findings of this study are available from the corresponding author upon reasonable request.

## REFERENCES

- K. Bertoldi, P. M. Reis, S. Willshaw, and T. Mullin, “Negative Poisson’s ratio behavior induced by an elastic instability,” *Adv. Mater.* **22**, 361–366 (2010).
- X. Zheng, H. Lee, T. H. Weisgraber, M. Shusteff, J. DeOtte, E. B. Duoss, J. D. Kuntz, M. M. Biener, Q. Ge, J. A. Jackson *et al.*, “Ultralight, ultrastiff mechanical metamaterials,” *Science* **344**, 1373–1377 (2014).
- T. Brunet, A. Merlin, B. Mascaró, K. Zimny, J. Leng, O. Poncelet, C. Aristégui, and O. Mondain-Monval, “Soft 3D acoustic metamaterial with negative index,” *Nat. Mater.* **14**, 384–388 (2015).
- Y. Wang, L. Li, D. Hofmann, J. E. Andrade, and C. Daraio, “Structured fabrics with tunable mechanical properties,” *Nature* **596**, 238–243 (2021).
- V. Zalipae, A. Movchan, C. Poulton, and R. McPhedran, “Elastic waves and homogenization in oblique periodic structures,” *Proc. R. Soc. London, Ser. A* **458**, 1887–1912 (2002).
- P. Wang, F. Casadei, S. H. Kang, and K. Bertoldi, “Locally resonant band gaps in periodic beam lattices by tuning connectivity,” *Phys. Rev. B* **91**, 020103 (2015).
- Z. Liu, X. Zhang, Y. Mao, Y. Zhu, Z. Yang, C. T. Chan, and P. Sheng, “Locally resonant sonic materials,” *Science* **289**, 1734–1736 (2000).
- Y. Chen, Z. Jia, and L. Wang, “Hierarchical honeycomb lattice metamaterials with improved thermal resistance and mechanical properties,” *Compos. Struct.* **152**, 395–402 (2016).
- L. R. Meza, A. J. Zelhofer, N. Clarke, A. J. Mateos, D. M. Kochmann, and J. R. Greer, “Resilient 3D hierarchical architected metamaterials,” *Proc. Natl. Acad. Sci.* **112**, 11502–11507 (2015).
- M. Miniaci, A. Krushynska, A. S. Gliozzi, N. Kherraz, F. Bosia, and N. M. Pugno, “Design and fabrication of bioinspired hierarchical dissipative elastic metamaterials,” *Phys. Rev. Appl.* **10**, 024012 (2018).
- S. H. Simon, *The Oxford Solid State Basics* (OUP, Oxford, 2013).
- K. H. Matlack, A. Bauhofer, S. Krödel, A. Palermo, and C. Daraio, “Composite 3D-printed metastructures for low-frequency and broadband vibration absorption,” *Proc. Natl. Acad. Sci.* **113**, 8386–8390 (2016).
- A. Palermo, S. Krödel, K. H. Matlack, R. Zacherini, V. K. Dertimanis, E. N. Chatzi, A. Marzani, and C. Daraio, “Hybridization of guided surface acoustic modes in unconsolidated granular media by a resonant metasurface,” *Phys. Rev. Appl.* **9**, 054026 (2018).
- P. Martakis, G. Aguzzi, V. K. Dertimanis, E. N. Chatzi, and A. Colombi, “Nonlinear periodic foundations for seismic protection: Practical design, realistic evaluation and stability considerations,” *Soil Dyn. Earthquake Eng.* **150**, 106934 (2021).
- R. Wiltshaw, J. M. De Ponti, and R. V. Craster, “Analytical solutions for Bloch waves in resonant phononic crystals: Deep subwavelength energy splitting and mode steering between topologically protected interfacial and edge states,” *arXiv:2207.13118* (2022).
- G. Ma and P. Sheng, “Acoustic metamaterials: From local resonances to broad horizons,” *Sci. Adv.* **2**, e1501595 (2016).
- M. Kadic, G. W. Milton, M. van Hecke, and M. Wegener, “3D metamaterials,” *Nat. Rev. Phys.* **1**, 198–210 (2019).
- A. Colombi, R. Zacherini, G. Aguzzi, A. Palermo, and E. Chatzi, “Mitigation of seismic waves: Metabarriers and metafoundations bench tested,” *J. Sound Vib.* **485**, 115537 (2020).
- J. Yu, C. Liu, C. Yang, B. Zhang, X. Zhang, and Y. Zhang, “Elastic wave attenuation in a functionally graded viscoelastic couple stress plate, sandwiched between two elastic half-spaces,” *Appl. Math. Modell.* **108**, 670–684 (2022).
- S. Tomita, H. Nishigaki, and R. Omote, “Elastic wave attenuation in a meta-plate with periodic hollow shapes for vibration suppression,” *J. Vib. Control* (published online 2022).
- C. Yilmaz, G. M. Hulbert, and N. Kikuchi, “Phononic band gaps induced by inertial amplification in periodic media,” *Phys. Rev. B* **76**, 054309 (2007).
- B. Van Damme, G. Hannema, L. Sales Souza, B. Weisse, D. Tallarico, and A. Bergamini, “Inherent non-linear damping in resonators with inertia amplification,” *Appl. Phys. Lett.* **119**, 061901 (2021).
- A. Colombi, D. Colquitt, P. Roux, S. Guenneau, and R. V. Craster, “A seismic metamaterial: The resonant metawedge,” *Sci. Rep.* **6**, 27717 (2016).
- N. Kaina, M. Fink, and G. Lerosee, “Composite media mixing Bragg and local resonances for highly attenuating and broad bandgaps,” *Sci. Rep.* **3**, 3240 (2013).
- A. O. Krushynska, M. Miniaci, F. Bosia, and N. M. Pugno, “Coupling local resonance with Bragg band gaps in single-phase mechanical metamaterials,” *Extreme Mech. Lett.* **12**, 30–36 (2017).
- L. J. Gibson and M. F. Ashby, *Cellular Solids: Structure and Properties* (Cambridge University Press, Cambridge, 1997).
- A. S. Phani, J. Woodhouse, and N. Fleck, “Wave propagation in two-dimensional periodic lattices,” *J. Acoust. Soc. Am.* **119**, 1995–2005 (2006).
- S. Krödel, T. Delpero, A. Bergamini, P. Ermanni, and D. M. Kochmann, “3D auxetic microlattices with independently controllable acoustic band gaps and quasi-static elastic moduli,” *Adv. Eng. Mater.* **16**, 357–363 (2014).
- G. Aguzzi, C. Kanellopoulos, R. Wiltshaw, R. V. Craster, E. N. Chatzi, and A. Colombi, “Octet lattice-based plate for elastic wave control,” *Sci. Rep.* **12**, 1088 (2022).
- E. Nolde, R. Craster, and J. Kaplunov, “High frequency homogenization for structural mechanics,” *J. Mech. Phys. Solids* **59**, 651–671 (2011).
- A. E. Miroshnichenko, S. Flach, and Y. S. Kivshar, “Fano resonances in nano-scale structures,” *Rev. Mod. Phys.* **82**, 2257 (2010).
- A. Bayat and S. Gaitanaros, “Wave directionality in three-dimensional periodic lattices,” *J. Appl. Mech.* **85**, 011004 (2018).
- J. Mueller, K. H. Matlack, K. Shea, and C. Daraio, “Energy absorption properties of periodic and stochastic 3D lattice materials,” *Adv. Theory Simul.* **2**, 1900081 (2019).
- X. Chen and H. Tan, “An effective length model for octet lattice,” *Int. J. Mech. Sci.* **140**, 279–287 (2018).
- J. A. Hawreliak, J. Lind, B. Maddox, M. Barham, M. Messner, N. Barton, B. Jensen, and M. Kumar, “Dynamic behavior of engineered lattice materials,” *Sci. Rep.* **6**, 28094 (2016).
- S. Krödel, A. Palermo, and C. Daraio, “Acoustic properties of porous microlattices from effective medium to scattering dominated regimes,” *J. Acoust. Soc. Am.* **144**, 319–329 (2018).
- G. Kim, C. M. Portela, P. Celli, A. Palermo, and C. Daraio, “Poroelastic microlattices for underwater wave focusing,” *Extreme Mech. Lett.* **49**, 101499 (2021).
- D. Beli, A. T. Fabro, M. Ruzzene, and J. R. F. Arruda, “Wave attenuation and trapping in 3D printed cantilever-in-mass metamaterials with spatially correlated variability,” *Sci. Rep.* **9**, 5617 (2019).
- A. Bergamini, M. Miniaci, T. Delpero, D. Tallarico, B. Van Damme, G. Hannema, I. Leibacher, and A. Zemp, “Tacticity in chiral phononic crystals,” *Nat. Commun.* **10**, 4525 (2019).
- T. Söderström and P. Stoica, *System Identification* (Prentice Hall International, 1989).
- I. Arretche and K. H. Matlack, “Experimental testing of vibration mitigation in 3D-printed architected metastructures,” *J. Appl. Mech.* **86**, 111008 (2019).
- S. Gonella, A. C. To, and W. K. Liu, “Interplay between phononic bandgaps and piezoelectric microstructures for energy harvesting,” *J. Mech. Phys. Solids* **57**, 621–633 (2009).



- <sup>43</sup>J. M. De Ponti, A. Colombi, R. Ardito, F. Braghin, A. Corigliano, and R. V. Craster, “Graded elastic metasurface for enhanced energy harvesting,” *New J. Phys.* **22**, 013013 (2020).
- <sup>44</sup>B. Zhao, H. R. Thomsen, J. M. De Ponti, E. Riva, B. Van Damme, A. Bergamini, E. Chatzi, and A. Colombi, “A graded metamaterial for broadband and high-capability piezoelectric energy harvesting,” *Energy Convers. Manage.* **269**, 116056 (2022).
- <sup>45</sup>S. Kirihaara, M. W. Takeda, K. Sakoda, and Y. Miyamoto, “Control of microwave emission from electromagnetic crystals by lattice modifications,” *Solid State Commun.* **124**, 135–139 (2002).
- <sup>46</sup>W. Dai, H. Wang, D. Zhou, Z. Shen, Y. Li, and D. Li, “The ultra-wide band gap property induced by lattice period gradually changing in three-dimensional photonic crystals,” *J. Am. Ceram. Soc.* **93**, 3980–3982 (2010).
- <sup>47</sup>N. Laforge, R. Wiltshaw, R. V. Craster, V. Laude, J. A. I. Martínez, G. Dupont, S. Guenneau, M. Kadic, and M. P. Makwana, “Acoustic topological circuitry in square and rectangular phononic crystals,” *Phys. Rev. Appl.* **15**, 054056 (2021).
- <sup>48</sup>S. Zhao, T. Feng, H. Zhang, Y. Gao, and Z. Chang, “Bloch wave propagation in finitely stretched soft lattice,” *Mech. Syst. Signal Process.* **181**, 109487 (2022).